Received: 22 January 2025 | Accepted: 21 April 2025

DOI: 10.1002/bmm2.70020

RESEARCH ARTICLE

BMEMat WILEY

Single-component cationic polyethylenimine thermogel for sustained and localized gene delivery to combat multi-drug resistant cancer

Qianyu Lin[1] | **Minting Liu**[2] | **Lingjie Ke**[2] | **Nicholas Wei Xun Ong**[1,3] | **Joey Hui Min Wong**[1] | **Cally Owh**[1,4] | **Valerie Ow**[1,4] | **Belynn Sim**[1,3] | **Yi Jian Boo**[1] | **Jason Y. C. Lim**[1,5] | **Yunlong Wu**[2] | **Xian Jun Loh**[1,3,5]

[1]Institute of Materials Research and Engineering (IMRE), Agency for Science, Technology and Research (A*STAR), Singapore

[2]Fujian Provincial Key Laboratory of Innovative Drug Target Research and State Key Laboratory of Cellular Stress Biology, School of Pharmaceutical Sciences, Xiamen University, Xiamen, China

[3]School of Materials Science and Engineering, Nanyang Technological University (NTU), Singapore

[4]Department of Biomedical Engineering, National University of Singapore (NUS), Singapore

[5]Department of Materials Science and Engineering, National University of Singapore (NUS), Singapore

Correspondence

Jason Y. C. Lim, Yunlong Wu and Xian Jun Loh.

Email: jason_lim@imre.a-star.edu.sg, wuyl@xmu.edu.cn and lohxj@imre.a-star.edu.sg

Funding information

Agency for Science, Technology and Research; IAF-PP grant, Grant/Award Number: H20c6a0033; National Research Foundation Singapore, Grant/Award Number: NRF-NRFI07–2021–0003; Natural Science Foundation of China, Grant/Award Number: 82173750

Abstract

Multi-drug resistant cancer cells with over-expression of Bcl2 anti-apoptotic proteins can be effectively killed by transfecting them with Nur77 transcription factor (pNur77). Previous attempts are generally therapeutically unsatisfactory due to low sustained gene expression and are further disadvantaged by their multi-component designs requiring complicated preparation. Herein, we designed a single cationic amphiphilic copolymer from branched poly(ethylenimine) (PEI-25k), the gold standard non-viral vector, that functions simultaneously as the non-viral vector and hydrogel forming polymeric matrix. Our single-component hydrogel gene delivery platform is highly facile to prepare as it only requires co-dissolution of the copolymer with pNur77 to form a homogeneous sol. Due to the high cationic charge density of PEI-25k, this PEI-based copolymer effectively complexes a high payload of the plasmid. Subsequently, the copolymer's thermogelling ability enables it to spontaneously self-assemble into a hydrogel depot by simply being warmed to physiological temperatures upon intra-tumoral injection. Leveraging upon the high transfection efficiency of PEI-25k, this PEI-based thermogel achieved prolonged localized release of pNur77 with high transfection efficiency. This leads to successful tumor size reduction and suppressed tumor reoccurrence in mouse models with low systemic cytotoxicity. We believe this single-component cationic thermogel non-viral gene delivery platform is highly attractive for gene therapy.

KEYWORDS

biocompatible, facile formulation, gene transfection, plasmid complexation, self-assembly, supramolecular hydrogels, temperature-responsive

Qianyu Lin and Minting Liu contributed equally to the study.

1 | INTRODUCTION

Cancer is a pathosis characterized by rapid uncontrolled proliferation of cells leading to the development of tumors.[1] It has been identified as the second highest contributor to mortality rate in developed countries after heart diseases.[2] Current clinical treatment of cancer commonly includes chemotherapy, which involves the administration of cytotoxic drugs orally or intravenously.[3] It is well known to be limited by non-specific drug distribution, poor drug solubility in physiological fluids, poor drug bioavailability, and rapid clearance of drug from bloodstream.[4] The effectiveness of chemotherapy is further reduced by multi-drug resistant (MDR) cancers, where cancer cells have enhanced ability to remove therapeutics via cellular pumps.[5] As such, it is of great urgency and high priority to develop alternative cancer treatment strategies that are effective against MDR cancers and have low side effects.[6]

Many cancers are caused by somatic mutations in upstream cell signaling pathways[7] or genetic lesions in genes that encode for cell cycle regulation proteins.[8] Together with early work that proved exogeneous genetic material can be integrated into human somatic cells to alter their cellular functions,[9] it has been proposed that gene therapy could be employed to correct the genetic lesions that first caused the onset of cancer.[10] Herein, we focus on MDR cancer that is associated with elevated expression of Bcl2 anti-apoptotic proteins as a disease model. Over-expression of these anti-apoptotic proteins prevents apoptosis by blocking the activation of Bak/Bax pro-apoptotic regulators.[11] We have selected to transfect the MDR cancer cells with pNur77 as it has been shown that Nur77 in the mitochondria is particularly effective at exploiting the overexpressed Bcl2 proteins to induce apoptosis by converting them from protectors to killers.[12] Nur77 interacts with Bcl2 through its ligand-binding domain, where Nur77 binds to the N-terminal loop region of Bcl2 located between its BH4 and BH3 structural domains, resulting in a conformational change that transforms Bcl2 from a protective protein to a killer protein.[13] As such, transfection of MDR cancer cells with pNur77 has been proposed as an effective strategy to combat MDR tumors.[12]

The ideal gene delivery vector should be able to encapsulate a high payload of genetic material,[14] achieve high transfection efficiency and sustained gene expression,[14,15] demonstrate high biocompatibility and allow for facile administration.[16] To date, many nanocarriers ranging from cationic polymers,[17] liposomes,[18] nanoparticles,[19] and viral vectors[20] have been explored for gene delivery due to their ability to complex or encapsulate anionic genetic material for subsequent transfection.[21] However, as these nanocarriers are commonly administered via injection into the body and allowed to undergo systemic circulation,[22] they often rely on enhanced permeation and retention effect associated with tumors[22] or tumor targeting receptors conjugated onto them to achieve accumulation at the tumor sites.[23] Despite these targeting strategies, the nanocarriers often struggle to achieve sufficient accumulation of genetic material at tumor sites to attain sustained gene expression for the desired therapeutic effect.[21,24]

Therefore, to achieve good therapeutic efficacy, it is essential to improve the localization of therapeutic genes.[25] To address this need, a myriad of injectable hydrogels has thus been developed where therapeutic genes are first complexed with vectors before being embedded in a secondary hydrogel matrix.[26] Here, we categorize this type of gene-hydrogel systems as two-component systems where the vector and hydrogel matrix are two distinct entities serving two separate functions (Table 1). A myriad of hydrogel encapsulated vectors are demonstrated in literature and include cationic polymers (such as linear poly(β-amino ester)[27] and polyethylenimine[30]), cationic amphipathic peptide,[28] adeno-associated virus vector,[29] and DNA-based vectors.[31] Preparation of these vectors and their complexes with the therapeutic genes are usually completed first before they are dispersed and embedded in an external hydrogel matrix made from a separate polymer such as hyaluronic acid,[27] chitosan,[28] gelatin,[29] polyethylene glycol,[30] and DNA-scaffold.[31] While many of these two-component hydrogel systems have been demonstrated to be effective at achieving sustained localized gene transfection with promising therapeutic outcomes, a two-component system is arguably complex as multiple steps are required to prepare the individual components before combining them.

To reduce the complexity of gene delivery hydrogel formulation, various research groups have attempted to design single-component systems where the gene vector is also the hydrogel matrix.[32,33] In other words, the vector complexes with the therapeutic gene and subsequently self-assemble into a hydrogel without additional crosslinkers. Such single-component hydrogel systems have been developed from nucleotides[33] or synthetic cationic polymers[32] capable of supramolecular self-assembly (Table 1). Ding et al. developed an RNA-triple-helix that was able to spontaneously self-assemble into a hydrogel[33]; this RNA-triple-helix was not only able to directly complex with the siRNA without the aid of additional cationic polymer vector but also able to act in synergy with the siRNA to achieve effective tumor abrogation and block metastasis.[33] While this strategy is highly promising, there is a significant challenge involved

TABLE 1 Classification of hydrogels for sustained and localized gene therapy.

S/N	No. of components	Vector	Hydrogel	Gene	Ref.
1	2	Linear poly(β-amino ester)	Hyaluronic acid	COL7A1	[27]
2	2	30-mer cationic amphipathic peptide (RALA)	Copolymer of deacetylated chitosan and N-isopropylacrylamide	pEGFP-N1	[28]
3	2	Recombinant adeno-associated virus (rAAV)	Gelatin	pAAV-IRES-hrGFP	[29]
4	2	Polyethyleneimine	Poly(ethylene glycol)-Fibrinogen (PF)	Antisense oligonucleotides (AONs)	[30]
5	2	"X"-shaped DNA scaffold	*I*-motif	Gaussia luciferase gene	[31]
6	1	Thermosensitive chitosan-*g*-poly(*N*-isopropylacrylamide)		Stomatin-like protein 2 (SLP2) short hairpin RNA (shRNA)	[32]
7	1	Polymerized RNA transcripts of miRNA-205, miRNA-221, and LXL apt-DNAChol		mRNA encoding *Gaussia* luciferase and enhanced green fluorescent protein	[33]

in the design of self-assembling triple helix to achieve synergistic therapeutic efficacy. A simpler and more versatile strategy would be to develop cationic polymers capable of self-assembly into hydrogel matrixes so that a wide variety of genetic payload can be facilely complexed within them. A chitosan-*g*-poly(*N*-isopropylacrylamide) (CPN) amphiphilic cationic copolymer was synthesized and complexed with stomatin-like protein 2 short hairpin RNA.[32] Being an amphiphilic thermogelling copolymer, CPN was able to undergo temperature responsive spontaneous sol-gel phase transition without additional crosslinkers,[32] thus demonstrating that it is an injectable, facile, and highly versatile single-component hydrogel gene delivery system.

While the chitosan-based thermogel system is a successful single-component gene delivery system, it is still constrained by its relatively low charge density, which can pose a limit on both the complexation of genetic material and subsequent transfection efficiency.[32] As such, we propose to improve the thermogel gene delivery system by increasing the cationic charge density by employing branched polyethylenimine (PEI = 25 kDa) as the hydrophilic segment of the thermogelling copolymer as it not only possesses high cationic charge density but is the gold standard amongst non-viral vectors.[34] Poly (propylene glycol) monobutyl ether (PPG-mbe) is selected as the hydrophobic segment as its lower critical solution temperature is near physiological temperature[35] and will allow us to easily tune the gelation temperature of the resultant thermogel by varying the PPG:PEI molar ratio.[36] Urethane linkages are used to conjugate PEI and PPG because it is relatively resistant to hydrolysis[37] which will grant the thermogel hydrolytic stability in vivo to achieve suitably long sustained release of the therapeutic gene. This PEI-PPG amphiphilic copolymer (named as gloPEI-mulPPG) forms micelles at low temperatures (10°C) which complexes with Nur77 nuclear transcription factor plasmid (pNur77) via simple mixing via electrostatic attraction between the cationic copolymer and anionic plasmid. This micellar solution undergoes spontaneous aggregation to form a localized gel depot upon warming to physiological temperatures after intra-tumoral injection into mouse models (Figure 1a) due to its thermogelling ability. Sustained release of pNur77 was achieved via the gradual erosion of the gloPEI-mulPPG gel depot. Compared to PEI-25 kDa gold standard, our gloPEI-mulPPG thermogel showed higher transfection efficiency, longer release duration, more effective tumor reduction and suppression of tumor reoccurrence. Lastly, we found that gloPEI-mulPPG thermogel exhibits minimal toxicity to key organs and the kidney during its residence lifetime in the body. Overall, we demonstrate that the gloPEI-mulPPG thermogel is a highly effective, versatile, biocompatible, and easy to formulate single-component formulation for gene therapy.

2 | RESULTS

2.1 | Synthesis and characterization

In this work, we designed a single PEI-based thermogelling copolymer that can simultaneously function as the non-viral vector to complex and deliver genetic material and as the hydrogel polymeric matrix. The gloPEI-mulPPG thermogelling copolymer was synthesized by covalent conjugation of hydrophobic poly(propylene

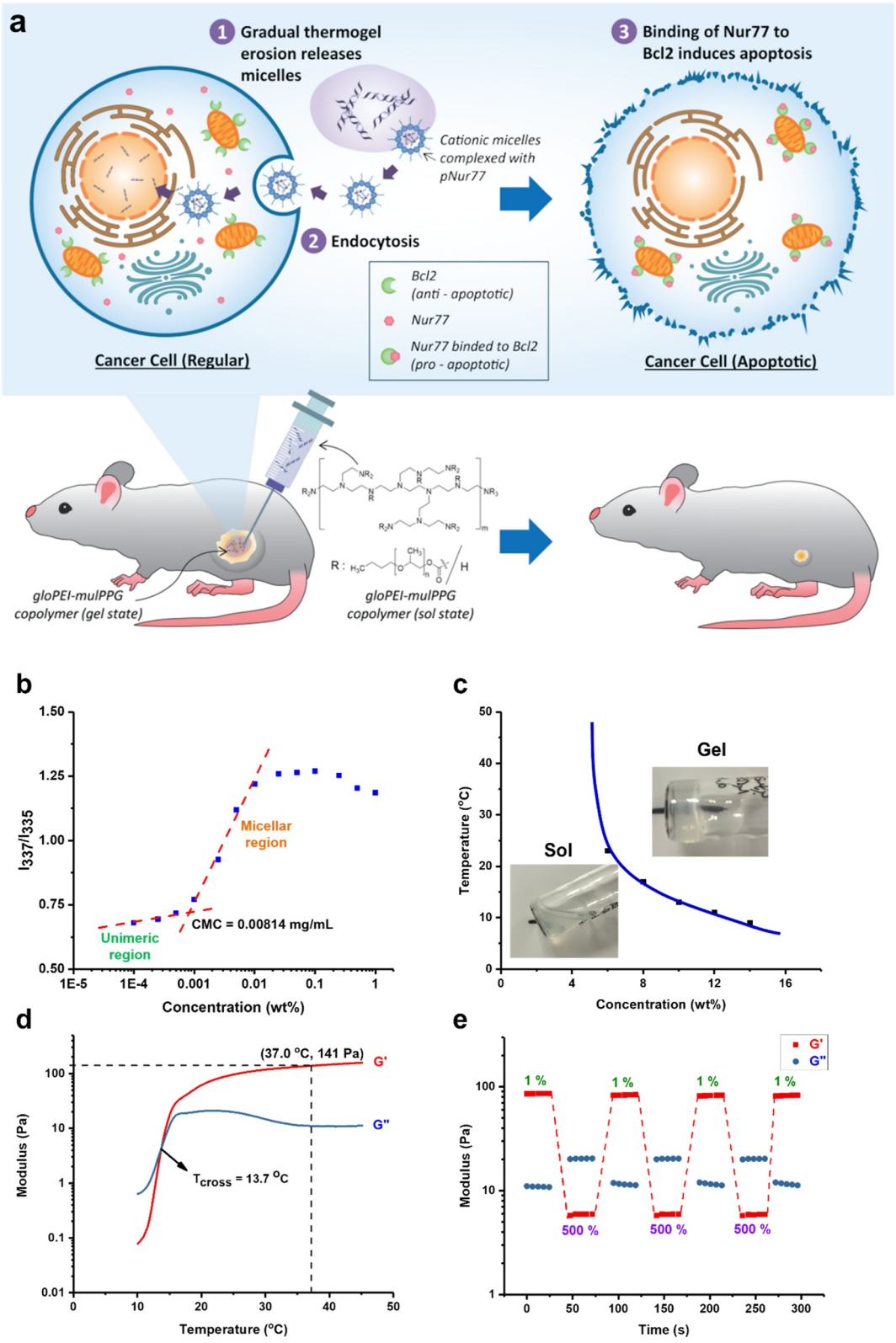

FIGURE 1 Overall schematic of cancer gene therapy by gloPEI-mulPPG thermogel and characterizations of gloPEI-mulPPG micelle and thermogel. (a) Schematic of cancer gene therapy by injecting gloPEI-mulPPG thermogel complexed with pNur77 into tumors to achieve sustained and localized transfection of multi-drug resistant cancer cells for effective shrinkage of tumor. (b) Plot of fluorescence emission intensity ratio at 337 nm to that of 335 nm against log(concentration). The intersection of best-fit lines of the unimeric and micellar regions gives the critical micelle concentration. (c) Temperature-concentration sol-gel phase diagram of gloPEI-mulPPG in deionized water. (d) Temperature-sweep rheological measurement at 3°C min^{-1} increment, 1% strain, and 1 Hz of gloPEI-mulPPG thermogel at prepared at 10 wt% in deionized water. (e) Time-sweep rheological measurement of PPG-PEI 10 wt% thermogel for 3 cycles of low strain (1%) and high strain (500%) at 37°C and 1 Hz.

glycol) mono butylether (PPG-mbe, 2.5 kDa) segments onto hydrophilic PEI-25k via urethane bond formation using 1,1′-carbonyldiimidazole (Supporting Information S1: Figure S1, see Methods for more details). ^{1}H nuclear magnetic resonance (NMR) spectroscopy of the isolated product showed unequivocal evidence of signals arising PEI and PPG protons (Supporting Information S1: Figure S2), whilst the presence of urethane linkages were determined from ^{13}C NMR ($\delta = 164$ ppm)[38] (Supporting Information S1: Figure S3) and Fourier transform infrared spectroscopy (FTIR) (urethane carbonyl stretch absorption peak at 1660 cm^{-1})[39] (Supporting Information S1: Figure S4). Successful covalent conjugation was further demonstrated using diffusion ordered spectroscopy (DOSY), showing a single diffusion coefficient of 5.12×10^{-12} cm^2 s^{-1} of both PPG and PEI components (Supporting Information S1: Figure S5), as well as from gel permeation chromatography (GPC) analysis that yielded a single peak (Supporting Information S1: Figure S6).

As the ability to form micelles capable of aggregating into thermogels[40] is essential for the gloPEI-mulPPG copolymer to function as a gene delivery hydrogel depot, we first ascertained its micelle forming ability in aqueous solution. Fluorescent pyrene molecules were introduced into gloPEI-mulPPG solutions and significant red shift of the emission spectrum was observed when they become encapsulated in the hydrophobic micelle cores at concentrations above the critical micelle concentration (CMC) (Supporting Information S1: Figure S7).[41] CMC was determined from the intersection of the unimeric and micellar regions and was thus found to be 0.00814 mg mL^{-1} (Figure 1b).[41] Thereafter, we proceeded to investigate the thermogelling behavior of gloPEI-mulPPG. Despite its polycationic character ($\zeta = +22.1 \pm 1.63$ mV), its critical gelation concentration (CGC) of 5 wt% (Figure 1c) is similar to many neutral thermogelling copolymers.[42] At concentrations above CGC, gloPEI-mulPPG solutions were able to undergo temperature-controlled reversible sol-gel phase transitions to form translucent hydrogels, with higher copolymer concentration resulting in lower gelation temperatures (Figure 1c). Rheological measurements confirmed the ability of gloPEI-mulPPG solutions to undergo temperature-triggered gelation: upon warming, both G′ and G'' increased sharply with G′ exceeding G'' at the crossover temperature (T_{cross}) of 13.7°C (Figure 1d), indicating that the gloPEI-mulPPG solution behaved more like an elastic solid (gel phase) rather than a viscous solution (sol phase) at temperatures > T_{cross}. This indicated that gloPEI-mulPPG could form a stable gel depot when warmed to physiological temperature in vivo.

To be used effectively as a gel depot for sustained gene delivery, the thermogel must be shear-thinning (i.e. injectable) to achieve minimal invasiveness during implantation,[43] yet not compromise on its viscoelastic properties after injection due to polymer chain degradation from the high shear forces encountered.[44] Thus, the shear-thinning properties of the gloPEI-mulPPG gel were confirmed by flow sweep measurements at 37°C, which showed that its viscosity decreased significantly as the shear rate increased (Supporting Information S1: Figure S8). Indeed, we also empirically determined that the 10 wt% gloPEI-mulPPG thermogel was easily injectable through medically-relevant 21 G needles. To demonstrate the possibility of thermogel viscoelastic self-recovery after injection, we performed time-sweep recovery experiments at 37°C where the 10 wt% thermogel was subjected to three cycles of low strain (1%) and high strain (500%)—the latter far exceeding the maximum applied strain of 63.0% where the gel reverted back into a sol ($G'' > G'$) (Supporting Information S1: Figure S9). As shown in Figure 1e, the gloPEI-mulPPG thermogel collapsed immediately upon application of 500% strain but reformed ($G' > G''$) when the applied strain was reduced to 1%. This occurred for all three cycles with minimal loss in the mechanical strength (G') of the thermogel after each round of high strain. This allows retention of the gloPEI-mulPPG thermogel viscoelastic properties as initially designed after injection. To further simulate the use case where cold sol (5°C) is injected into a tumor (37°C), time sweep oscillatory measurements were performed and results showed that gloPEI-mulPPG was able to reach its maximum gel stiffness within ~20 s upon exposure to physiological temperatures (Supporting Information S1: Figure S10). This rapid gelation is advantageous as it minimizes the loss of encapsulated plasmids due to dilution by bodily fluids upon injection.

2.2 | In vitro biocompatibility and complexation with pNur77

In addition to facile gelation and injectability, it is essential for the gloPEI-mulPPG thermogel to demonstrate excellent biocompatibility and high payload carrying capacity for its application as a sustained gene delivery platform.[45] We first compared the biocompatibility of gloPEI-mulPPG and PEI-25k across three cell lines, namely healthy HEK293T cell line (Figure 2a), hepatocellular carcinoma HepG2 cell line (Figure 2b), and drug-resistant hepatocellular carcinoma HepG2-Bcl2 cell line (Figure 2c). Our results showed that cell viabilities were significantly higher when incubated with gloPEI-mulPPG as compared to PEI-25k across all three cell lines.

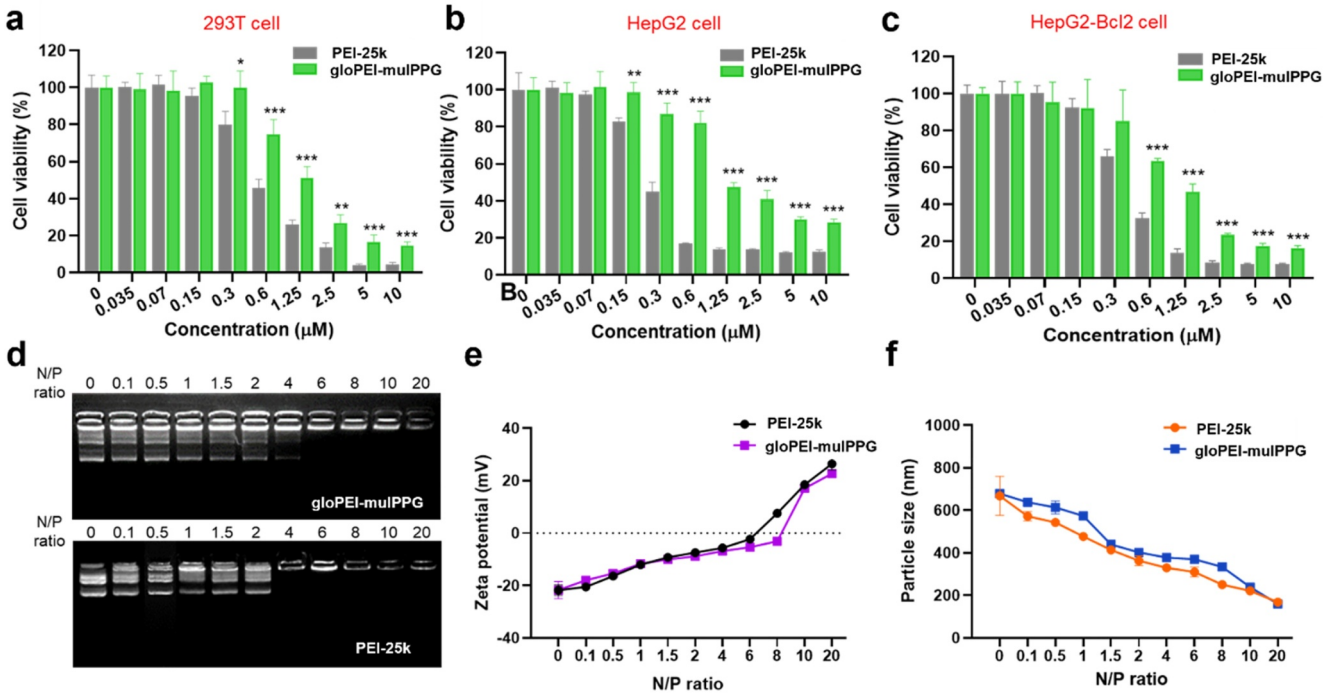

FIGURE 2 In vitro biocompatibility of gloPEI-mulPPG and characterizations of its complexes with pNur77. Cell viability of (a) 293T cells, (b) HepG2 cells, and (c) HepG2-Bcl2 cells after 24 h exposure to gloPEI-mulPPG and PEI-25k as measured by methylthiazolyldiphenyl-tetrazolium bromide assay. (d) Gel-retardation experiments ($n = 4$) on gloPEI-mulPPG and PEI-25k complexed with pNur77 at various N/P ratios. (e) Zeta potentials and (f) particle sizes of gloPEI-mulPPG/pNur77 and PEI-25k/pNur77 at various N/P ratios ($n = 3$). Data were plotted as mean ± standard deviation. Statistical significance was calculated by unpaired *t*-test where $^{*}p < 0.05$, $^{**}p < 0.01$, and $^{***}p < 0.001$.

Due to the basicity of amine groups on both gloPEI-mulPPG and PEI-25k, both are cationic polymers in aqueous solution and can be readily complexed with anionic genetic material via electrostatic adsorption. Their capacities to carry genetic material were measured by gel retardation experiments (Figure 2d), which showed that pNur77 was fully combined with gloPEI-mulPPG and PEI-25k at N/P ratios of 6 and 4, respectively, indicating the slightly higher gene loading capacity of PEI-25k. This was corroborated by zeta potential measurements, which showed that neutral complexes with pNur77 could be formed by gloPEI-mulPPG and PEI-25k at N/P ratios of 8 and 6, respectively (Figure 2e). Expectedly, higher plasmid loadings (N/P ratio) also resulted in reduction in the size of polymer-plasmid complexes (Figure 2f).

2.3 | In vitro transfection efficacies

For the gloPEI-mulPPG thermogel to be an effective gene delivery platform, it must demonstrate high transfection efficiency for therapy. We first evaluated the in vitro transfection efficiencies of gloPEI-mulPPG and PEI-25k by complexing them with Nur77-green fluorescent protein (Nur77-GFP) gene segment at various N/P ratios before incubating them with HEK293T cells. Since successful transfection will lead to the production of GFP in the cells, the transfection efficiencies of the polymers can be visualized (Figure 3a) and subsequently semi-quantified (Figure 3b) via confocal microscopy. Our results demonstrated that gloPEI-mulPPG achieved significantly higher transfection efficiency than PEI-25k at most of the tested N/P ratios and the highest transfection efficiency of ~60% was achieved for gloPEI-mulPPG at a N/P ratio of 20 (Figure 3b).

The transfection efficiencies of gloPEI-mulPPG copolymer and PEI-25k were further quantified using the Renilla luciferase assay. pRL-Renilla was complexed with gloPEI-mulPPG and PEI-25k at various N/P ratios before being incubated with HEK293K cells. Like the earlier Nur77-GFP results, luciferase expression levels increased for both gloPEI-mulPPG and PEI-25k with an increased N/P ratio (Figure 3c). While results showed that the luciferase expression levels were similar between gloPEI-mulPPG and PEI-25k at most of tested N/P ratios (Figure 3c; Supporting Information S1: Figures S11 and S12), gloPEI-mulPPG copolymer is still

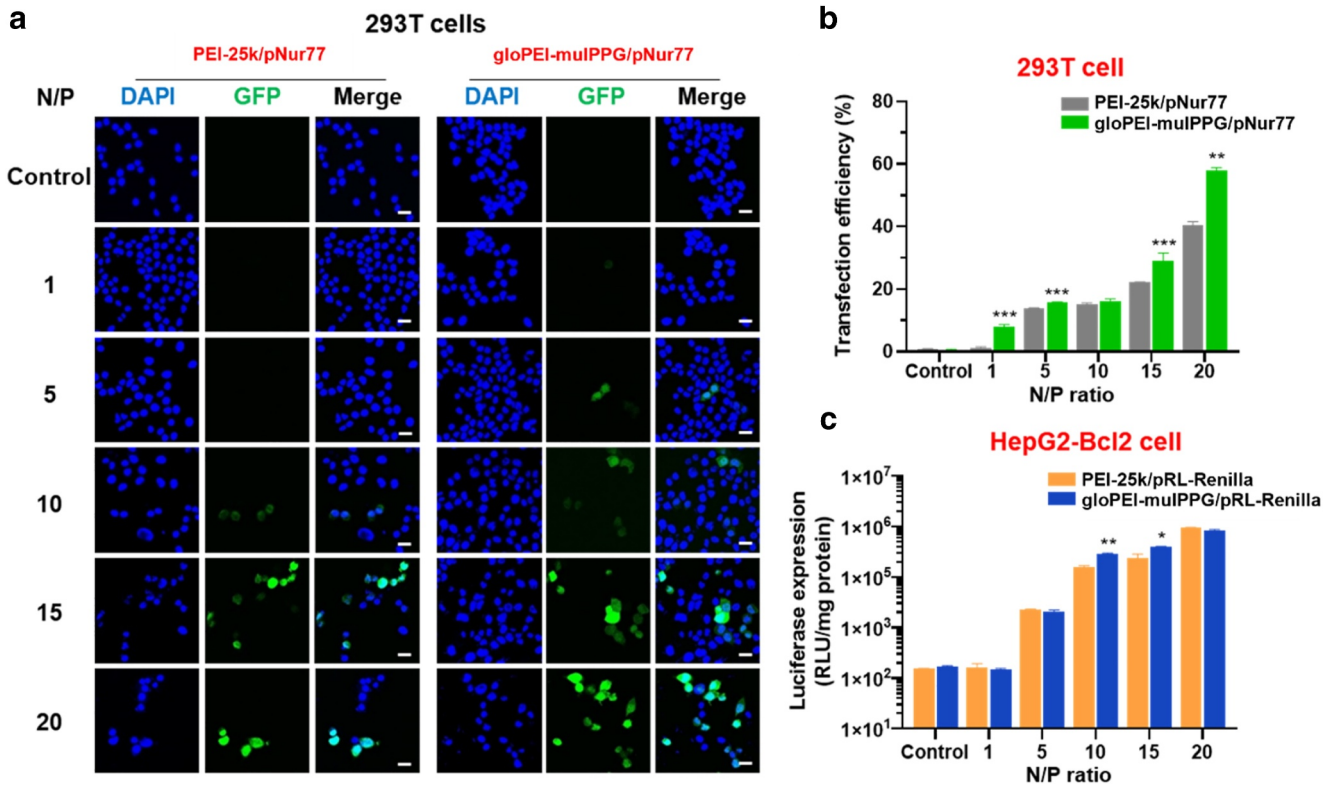

FIGURE 3 Transfection efficiency of gloPEI-mulPPG compared to that of PEI-25k gold standard. (a) Representative confocal microscopy images of HEK293T cells transfected with Nur77-GFP gene using gloPEI-mulPPG copolymer and PEI-25k at N/P ratios ranging from 1 to 20. The nuclei were visualized with DAPI and the Nur77 proteins were observed by their green fluorescence. (b) Transfection efficiencies of gloPEI-mulPPG copolymer and PEI-25k as quantified based on representative confocal images ($n = 3$). (c) Luciferase expression levels in HEK293T cells after being transfected with pRL-Renilla that was complexed with gloPEI-mulPPG copolymer and PEI-25k at N/P ratios ranging from 1 to 20 ($n = 3$). Data points are plotted as mean values ± standard deviation. Statistical significance was calculated by unpaired *t*-test where $^{*}p < 0.05$, $^{**}p < 0.01$, and $^{***}p < 0.001$. Nur77-GFP, Nur77-green fluorescent protein.

superior to PEI-25k due to its improved biocompatibility.

2.4 | In vitro therapeutic efficacies

The goal of gloPEI-mulPPG thermogel as a gene delivery platform is to achieve improved therapeutic efficacy against MDR cancer. As such, we proceeded to evaluate the in vitro potency of gloPEI-mulPPG/pNur77 against HepG2-Bcl2 cells. HepG2-Bcl2 were incubated with naked pNur77, PEI-25k/pNur77, and gloPEI-mulPPG/pNur77 at increasing concentrations of pNur77 for 24 h before the respective cell viabilities were quantified via methylthiazolyldiphenyl-tetrazolium bromide (MTT) assay. At low concentrations of pNur77 (<1 μg mL^{-1}), all three treatment methods were ineffective in inducing apoptosis in HepG2-Bcl2 cells (Figure 4a). While exposing HepG2-Bcl2 cells to higher concentrations of naked pNur77 remained ineffective at inducing apoptosis (cell viability remained >80% at 8 μg mL^{-1} of pNur77), gloPEI-mulPPG/pNur77 was able to achieve significantly higher cytotoxicity against HepG2-Bcl2 cells with cell viability being reduced to ~50% with 8 μg mL^{-1} of pNur77. In comparison, PEI-25k/pNur77 showed ~60% cell viability with 8 μg mL^{-1} of pNur77 (Figure 4a). This indicated that gloPEI-mulPPG was more effective against MDR cancer cells than PEI-25k.

Transfection of pNur77 leads to the production of Nur77 proteins in the cell, which bind readily to Bcl2 proteins (named as Bcl2-BH3), thereby activating the apoptotic pathway. As such, to compare the efficacies of the various treatments, Western Blot analysis was performed to visualize (Figure 4b; Supporting Information S1: Figures S14 and S15) and quantify (Figure 4c) the amount of Bcl2-BH3 protein present in HEK293T cells. The results showed that gloPEI-mulPPG/pNur77 produced significantly more Bcl2-BH3 proteins than PEI-25k/pNur77 and naked pNur77 (Figure 4b,c). This indicated that it is essential for the naked pNur77 to be complexed by a polymeric vector to achieve improved gene expression and gloPEI-mulPPG is more effective than PEI-25k as a gene delivery vector.

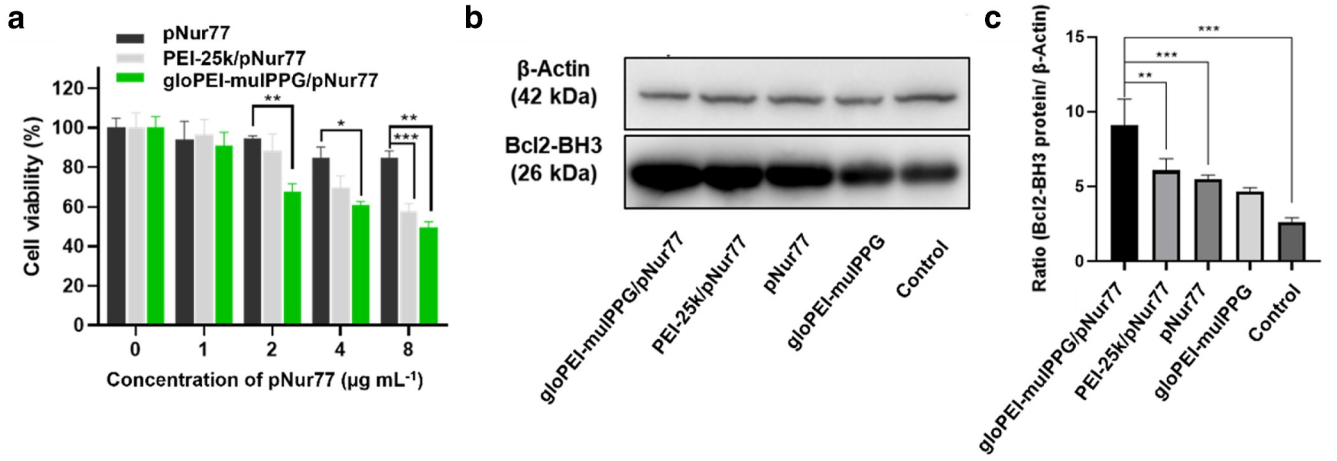

FIGURE 4 In vitro evaluation of therapeutic efficiencies after exposing HepG2-Bcl2 cells to pNur77 using various gene delivery vectors. (a) Cell viability after incubation with naked pNur77, gloPEI-mulPPG/pNur77, and PEI-25k/pNur77 at increasing pNur77 complexation concentrations ($n = 4$). (b) Representative Western Blot image for visual comparison of Bcl2-BH3 production in transfected cells after three different delivery strategies ($n = 4$); gloPEI-mulPPG/pNur77 and PEI-25k/pNur77 were formulated at N/P ratio of 20. (c) Semi-quantitative evaluation of Bcl2-BH3 protein production in cells using the Western Blot images obtained ($n = 4$). Data are presented as mean ± standard deviation. Statistical significance was calculated by ordinary one-way ANOVA with Tukey's post hoc test with $^{*}p < 0.05$, $^{**}p < 0.01$, and $^{***}p < 0.001$. ANOVA, analysis of variance.

2.5 | Release profile of pNur77 from gloPEI-mulPPG and its therapeutic efficacy

In addition to having good transfection and potency towards MDR cancer cells, it is crucial for gloPEI-mulPPG thermogel to demonstrate gradual erosion accompanied with sustained release of pNur77 to achieve prolonged on-site localized transfection for enhanced therapeutic effectiveness. Therefore, we proceeded to record the release profile of pNur77 from a formulation of 10 wt% gloPEI-mulPPG thermogel with plasmid loading at N/P = 20, into an equal volume of phosphate buffer above the thermogel depot (Figure 5a). Our results showed that the gloPEI-mulPPG thermogel was capable of sustained release of pNur77 with ~80% being released over 6 days (Figure 5b). Further analysis suggested that the release kinetics can be well-modeled by the Korsmeyer-Peppas power law.[46] It is found that the release exponent is 0.461 (Supporting Information S1: Figure S13), which indicates that the release mechanism is dominated by swelling and erosion of the hydrogel depot assuming that the depot has a cylindrical geometry in the in vitro set-up.[46] This can be plausibly attributed to the strong electrostatic interactions that exist between the cationic PEI-based thermogelling copolymers and anionic plasmid, which potentially retarded the rate of diffusion of the plasmid out of the hydrogel depot. Additionally, we showed that the daily-released pNur77 remained bioactive for cell apoptosis in HepG2-Bcl2 cells for the entire duration (Figure 5c). This suggested that the eroded micelles were able to protect pNur77 and enabled efficient transfection over a prolonged period. This indicated that gloPEI-mulPPG/pNur77 thermogel had potential to achieve sustained gene expression and thus enhanced therapeutic effectiveness.

In vivo erosion of the gloPEI-mulPPG thermogel was then probed by fluorescence imaging using a fluorescein isothiocyanate (FITC)-encapsulated thermogel injected into a mouse model (Figure 5d,e). With the gloPEI-mulPPG thermogel, the fluorescent area shrunk over time but remained detectable for 8 days, whilst the signal from PEI-25k/FITC was only detectable for 2 days (Figure 5e). This is clear evidence that the gloPEI-mulPPG thermogel had enhanced erosion resistance as compared to PEI-25k, enabling it to function as a sustained gene delivery platform.

2.6 | In vivo therapeutic efficacy

With earlier in vitro studies demonstrating sustained release of pNur77 from gloPEI-mulPPG thermogel and its potency towards HepG2-Bcl2 cells, we proceeded to evaluate the in vivo therapeutic effectiveness of gloPEI-mulPPG/pNur77 in nude mice models. 30 nude mice were randomly grouped into groups of five before HepG2-Bcl2 cells were subcutaneously injected into each mouse near its right hind leg to form tumors. As the solid tumors grew and reached approximately 100 mm^3, 100 μL of various treatment formulations (namely

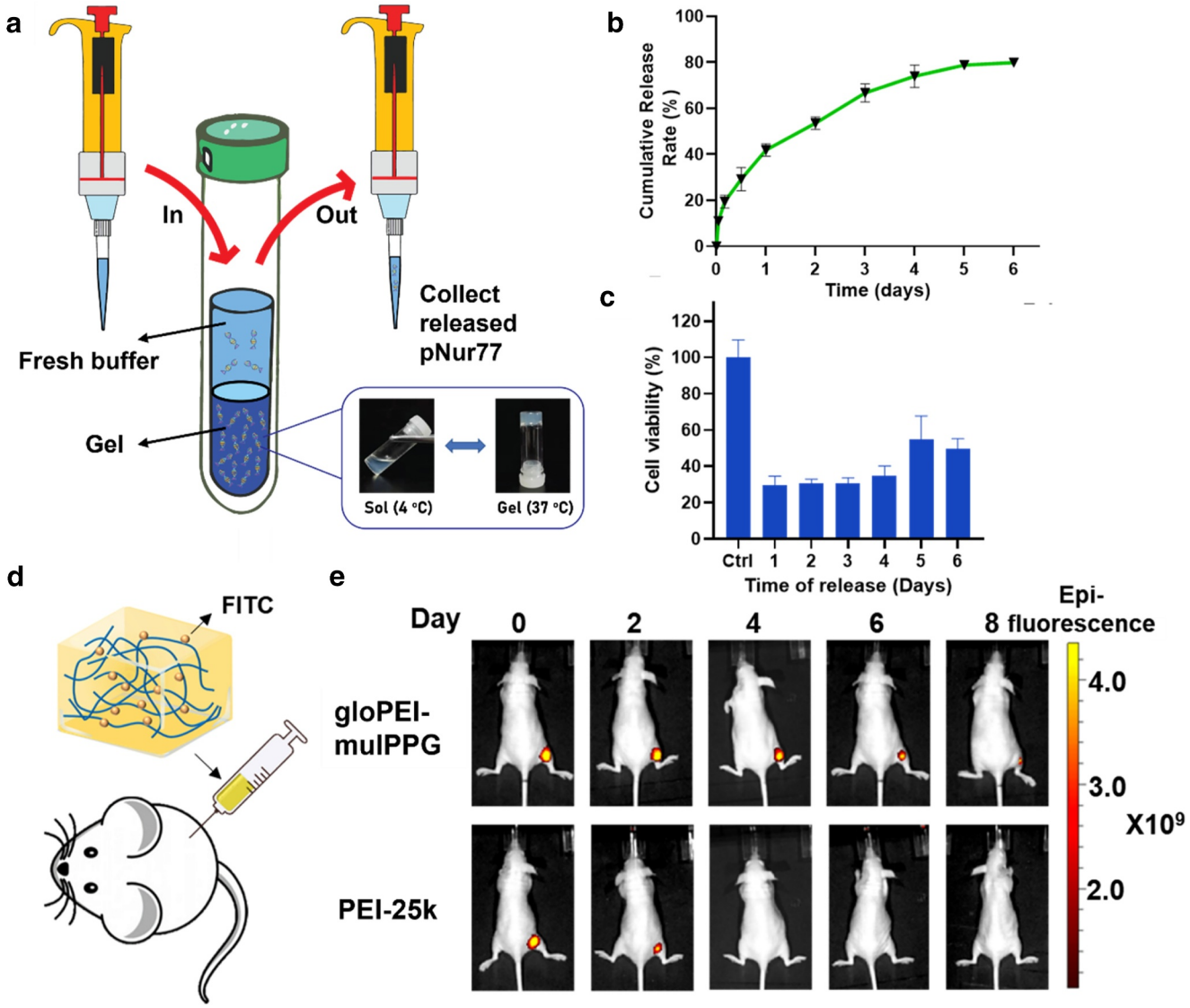

FIGURE 5 Gradual erosion of gloPEI-mulPPG thermogel accompanied by sustained release of pNur77. (a) In vitro experimental set-up to collect and quantify the amount of the released pNur77 from gloPEI-mulPPG thermogel. (b) Cumulative amount of pNur77 released over 6 days ($n = 3$). (c) Cell viability of HepG2-Bcl2 cells determined via methylthiazolyldiphenyl-tetrazolium bromide assay after 24 h incubation with eroded gloPEI-mulPPG/pNur77 micelles collected on different days ($n = 4$). (d) Schematic showing the encapsulation of fluorescein isothiocyanate (FITC) into gloPEI-mulPPG thermogel and PEI-25k solution followed by subcutaneous injection into mouse models. (e) In vivo observation of the erosion rates of gloPEI-mulPPG/FITC thermogel and PEI-25k/FITC by using fluorescence imaging. Data are plotted as mean values ± standard deviation.

phosphate buffered saline [PBS], naked pNur77, PEI-25k, gloPEI-mulPPG, PEI-25k/pNur77, and gloPEI-mulPPG/pNur77) were injected intratumorally every 6 days with pNur77 loading being constant at 0.15 mg mL^{-1} across the various treatments.

Nude mice implanted with HepG2-Bcl2 solid tumors from each treatment group were photographed after 14 days (Figure 6a) and treatment with gloPEI-mulPPG/pNur77 appeared to achieve the smallest tumor size, followed by treatment with PEI-25k/pNur77 and naked pNur77, respectively. This was further confirmed from the photo of the excised tumors (Figure 6b). The rate of tumor growth in each treatment group was tracked for 14 days, showing that gloPEI-mulPPG/pNur77 achieved the slowest tumor growth with the final average size of tumor being 261 ± 81 mm^3, which was significantly smaller than all other groups (Figure 6c). Between PEI-25k/pNur77 and naked pNur77, the former was able to achieve significantly smaller tumor sizes. In contrast, control experiments showed that treatment with saline, PEI-25k, and gloPEI-mulPPG without pNur77 led to rapid tumor growth.

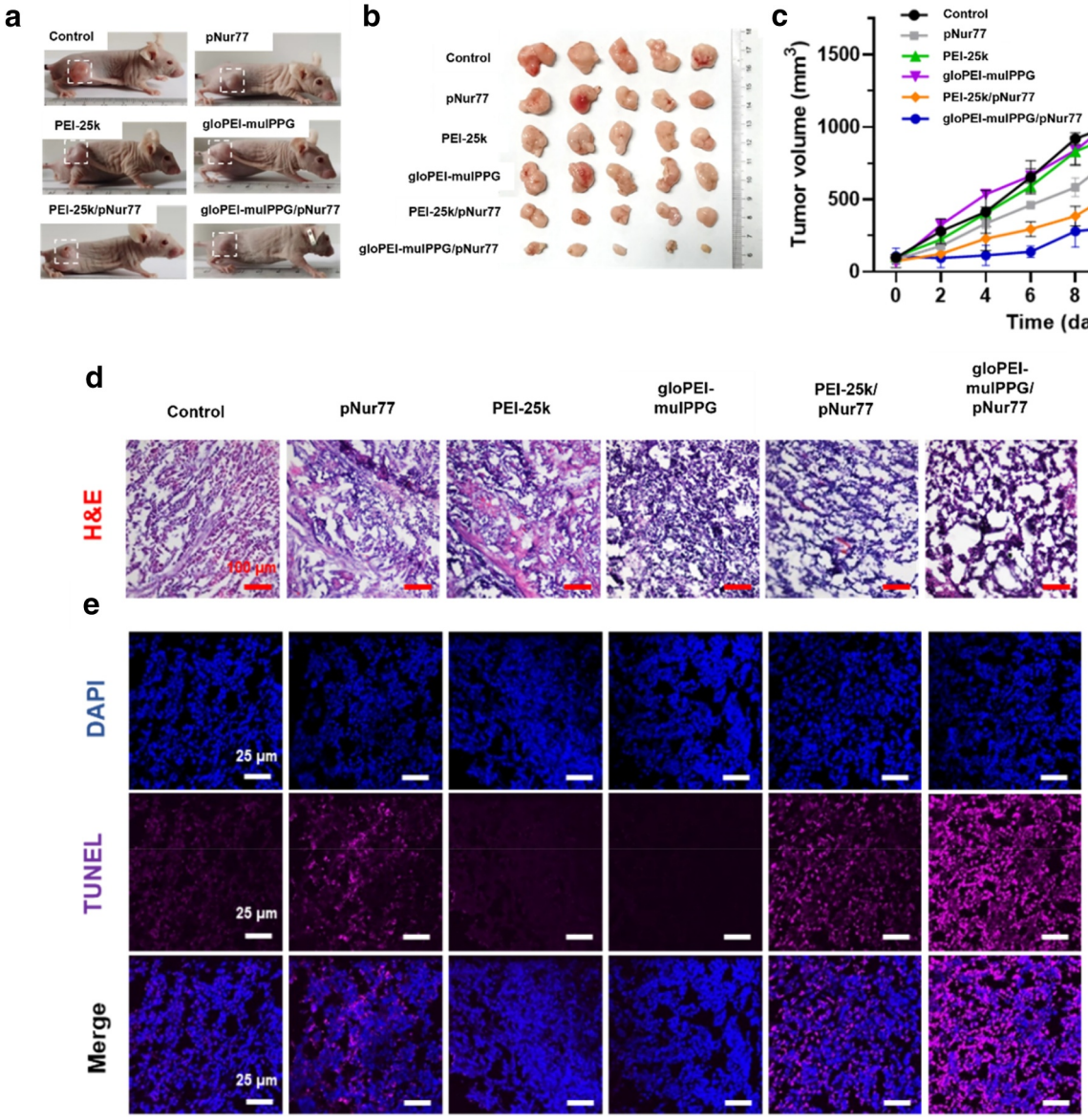

FIGURE 6 In vivo therapeutic efficacy of gloPEI-mulPPG/pNur77 against multi-drug resistant tumor models in mice. (a) Photos of representative nude mouse models implanted with HepG2-Bcl2 tumors after 14 days of various treatments, namely intra-tumoural injection of saline, naked pNur77, PEI-25k, gloPEI-mulPPG, PEI-25k/pNur77, and gloPEI-mulPPG/pNur77 where pNur77 loading was constant at 0.15 mg mL^{-1} across the treatments. (b) Photographs of representative tumors excised from nude mouse models that were euthanized after 14 days of treatment. (c) Tumor volumes in nude mice of each treatment group was recorded every 2 days during the treatment period ($n = 5$). Data were plotted as mean ± standard deviation and statistical significance was calculated by ordinary one-way ANOVA with Tukey's post hoc test where $^{**}p < 0.01$ and $^{***}p < 0.001$. Representative images of excised tumor tissue after (d) H&E staining and (e) TUNEL/DAPI staining. ANOVA, analysis of variance.

The tumors were excised from the mouse models after 14 days of treatment and representative sections were fixed and stained. Hematoxylin-eosin (H&E) staining showed obvious necrosis of tumor tissue after treatment with gloPEI-mulPPG/pNur77 with large and numerous pores being observed in the section (Figure 6d). This was congruent with the slow tumor growth observed earlier. In comparison, smaller pores were observed in the tumor sections obtained from the groups treated with PEI-25k/pNur77 and naked pNur77 (Figure 6d), indicating less necrotic tissue in these two groups, thus accounting for the more rapid tumor growth in these two groups. Lastly, tumor sections obtained from groups treated with PEI-25k and gloPEI-mulPPG without pNur77 appeared to cause minimal tumor necrosis (Figure 6d), indicating that the polymeric vectors themselves did not possess therapeutic effectiveness.

Terminal deoxynucleotidyl transferase-mediated dUTP nick end labeling (TUNEL) assay was employed to complement H&E staining (Figure 6e). TUNEL assay detects DNA fragmentation by labeling free 3′-hydroxyl termini with a fluorescent probe to visualize cell apoptosis.[47] The strongest fluorescence was observed from the tumor tissue of the gloPEI-mulPPG/pNur77 treatment group, followed by PEI-25k/pNur77 and naked pNur77. This indicated that gloPEI-mulPPG/pNur77 achieved the highest cell apoptosis rate. Taken together, the results were conclusive that gloPEI-mulPPG/pNur77 showed the best therapeutic effectiveness, successfully inhibiting tumor growth by causing significant tumor cell apoptosis and tissue necrosis.

2.7 | Biocompatibility towards key organs

In addition to therapeutic effectiveness, an ideal gene delivery platform should exhibit low systemic toxicity. As such, the in vivo biocompatibilty of gloPEI-mulPPG thermogel was investigated by examining tissue sections from key organs obtained from the euthanized mice models after H&E staining. The histomorphologies of the heart, liver, spleen, lung, and kidney tissues all appeared healthy and normal across all treatment groups (Figure 7a). This suggested that both PEI-25k and gloPEI-mulPPG could be considered as safe and biocompatible gene delivery vectors.

The biocompatibility of PEI-25k and gloPEI-mulPPG was further evaluated by investigating the liver and kidney functions of the mice after treatment. Being responsible for clearing the polymeric vectors from the body, they can be susceptible to polymer-induced damage. The liver and kidney functions were evaluated by measuring the levels of alkaline phosphate (ALP), aspartate transferase (AST), alanine aminotransferase (ALT), blood urea nitrogen (BUN) and blood albumin (ALB) in their blood serum (Figure 7b).[48] The ALP serum level was significantly lowered after the mice models were exposed to PEI-25k and PEI-25k/pNur77. Since unusual levels of

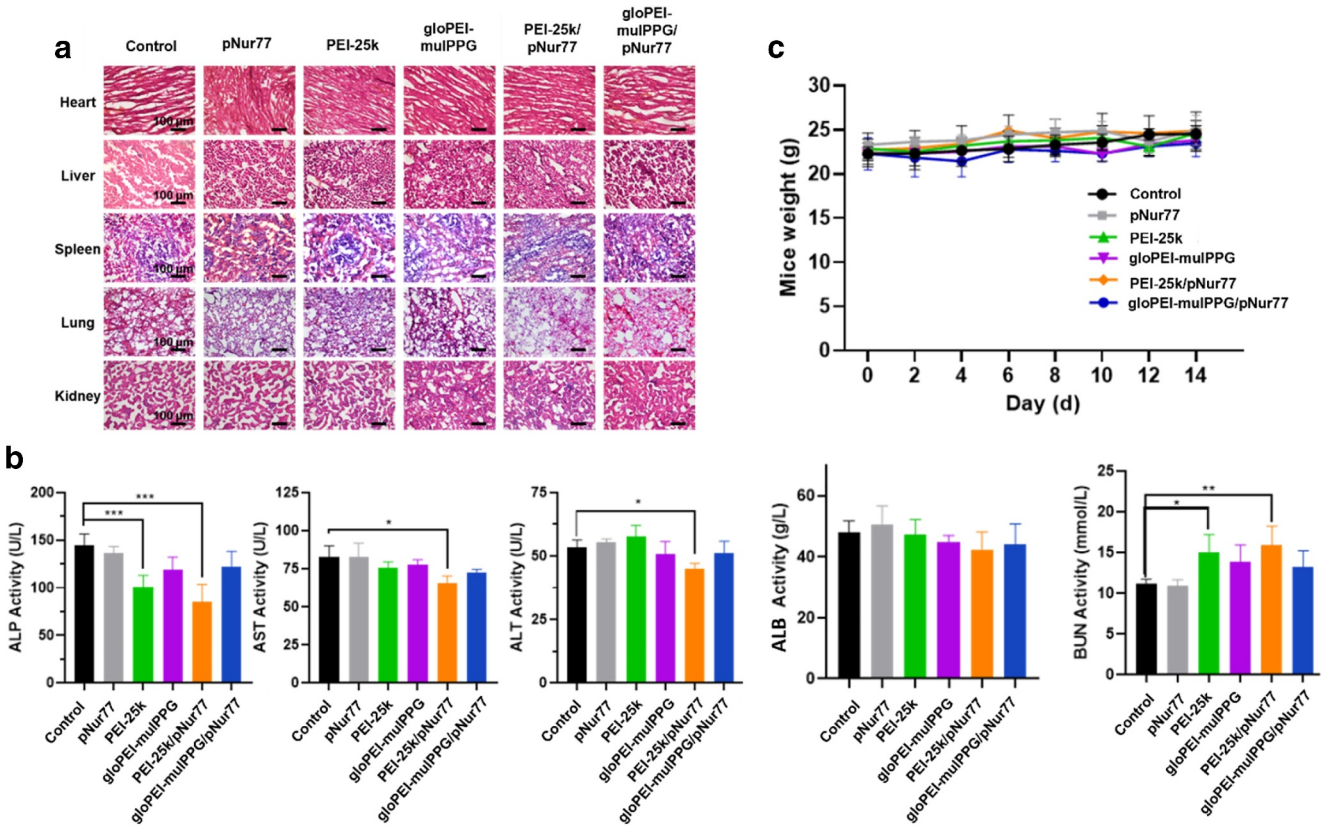

FIGURE 7 In vivo biocompatibility evaluation of the various treatments after 14 days. (a) Representative H&E images of tissues obtained from the heart, liver, spleen, lung, and kidney of euthanized mice after various treatments. (b) Biochemical indices of the livers (ALP, AST, ALT, ALB) and kidneys (BUN) of mice models after various treatments ($n = 5$). Data are expressed as mean ± standard deviation. Statistical significance was calculated by ordinary one-way ANOVA with Tukey's post hoc test, where $^{*}p < 0.05$, $^{**}p < 0.01$, and $^{***}p < 0.001$. (c) Weight of mice models subjected to different treatments over 2 weeks. ALB, albumin; ALP, alkaline phosphate; ALT, alanine aminotransferase; ANOVA, analysis of variance; AST, aspartate transferase; BUN, blood urea nitrogen.

ALP is an indicator for underlying liver problems,[49] this result suggested that both PEI-25k and PEI-25k/pNur77 plausibly compromised the liver health of the mice models. In contrast, normal ALP levels were found in mice models implanted with gloPEI-mulPPG and gloPEI-mulPPG/pNur77.

Although ALP levels indicated that PEI-25k posed some toxicity to the liver, the negative impact appeared to be relatively mild. Damaged cells are known to leak AST and ALT into the bloodstream and cause elevated AST and ALT levels.[49,50] Since the AST and ALT levels of mice exposed to PEI-25k, PEI-25k/pNur77, gloPEI-mulPPG, and gloPEI-mulPPG/pNur77 were all found to be not significantly higher than the control group, this indicated that none of the treatments caused significant cytotoxicity to the liver. This was further corroborated by ALB levels. ALB is produced in the liver and is essential to the health of blood vessels; a low ALB level is thus indicative of reduced liver function.[51] The results showed that none of the treatments led to significantly lowered ALB levels, therefore this suggested that both PEI-25k and gloPEI-mulPPG did not pose significant toxicity to the liver.

The kidney health of the mouse models was evaluated by measuring the BUN levels (Figure 7b). While the liver metabolizes proteins and releases BUN into the bloodstream, the kidney works to extract BUN from the blood and excrete it.[52] A high level of BUN would indicate reduced kidney function as they are struggling to remove BUN.[52] Our results showed that PEI-25k and PEI-25k/pNur77 led to significantly higher BUN levels, suggesting that PEI-25k compromised kidney function and thus had the potential to cause other health conditions associated with weaker kidney function. In contrast, gloPEI-mulPPG and gloPEI-mulPPG/pNur77 both showed comparable BUN levels with respect to the control group, indicating that gloPEI-mulPPG did not significantly reduce kidney function.

Finally, the body weights of the mice models were monitored during treatment. It was observed that their body weights remained relatively constant and comparable across the various treatment groups (Figure 7c). This suggested that none of the treatments caused significant changes in the feeding and activity patterns of the mice that might lead to large fluctuations in body mass. Taken together, our results suggested that both PEI-25k and gloPEI-mulPPG did not cause acute systemic toxicity to the mice. However, PEI-25k plausibly posed slight toxicity towards the liver and further caused reduced kidney function. In comparison, gloPEI-mulPPG showed better biocompatibility with no significant damage to both liver and kidneys.

2.8 | Suppressing tumor re-growth

Clinical treatment of cancer commonly includes surgical removal of tumors as a key intervention step to slow tumor growth. However, it is impossible to completely remove tumors surgically, allowing for tumor regrowth from the remnant cancerous tissue. Thus, GloPEI-mulPPG/pNur77 should suppress tumor regrowth to be an effective cancer treatment. To study this possibility, mouse models bearing recurrent tumors were established: Mice were randomly grouped into threes and inoculated with HepG2-Bcl2 cells to initiate tumor growth (Figure 8a). As tumor volume approached 300 mm^3, 98% of the tumor volume in each mouse was surgically removed. This was followed by the application of the various treatments to the excised tumor sites. Their effectiveness at inhibiting tumor regrowth was evaluated by comparing the tumor sizes after 22 days (Figure 8b,c).

Mouse models bearing recurrent tumors were established to compare the effectiveness of various treatment strategies for suppressing tumor re-growth. Mice were randomly grouped into threes and inoculated with HepG2-Bcl2 cells to initiate tumor growth (Figure 8a). As tumor volume approached 300 mm^3, 98% of the tumor volume in each mouse was surgically removed. This was followed by the application of the various treatments to the excised tumor sites (Figure 8a). Their effectiveness at inhibiting tumor regrowth was evaluated by comparing the tumor sizes after 22 days (Figure 8b,c).

From visual observation of the excised recurrent tumors, it was apparent that gloPEI-mulPPG/pNur77 achieved the smallest tumors followed by PEI-25k/pNur77 (Figure 8b). This was further corroborated by tracking tumor volume between Day 7 and Day 22 (Figure 8c). The graph showed that tumor growth was significantly slower in mice implanted with gloPEI-mulPPG/pNur77 as compared to mice treated with PEI-25k/pNur77. The recurrent tumors were excised and subjected to H&E staining. The results showed obvious tumor tissue necrosis when treated with gloPEI-mulPPG/pNur77 (Figure 8e), which accounted for the suppressed tumor regrowth. In comparison, less necrotic tissue was observed in the group treated with PEI-25k/pNur77 (Figure 8e), which could account for the significant tumor regrowth observed. These results suggested that gloPEI-mulPPG/pNur77 had significantly higher effectiveness than PEI-25k/pNur77 in suppressing tumor regrowth. Finally, we again found that there were no significant changes in body weights of mice across the different treatment groups (Figure 8d). This suggested that the polymeric vectors and their complexes with pNur77 did not pose acute toxicity to the mice.

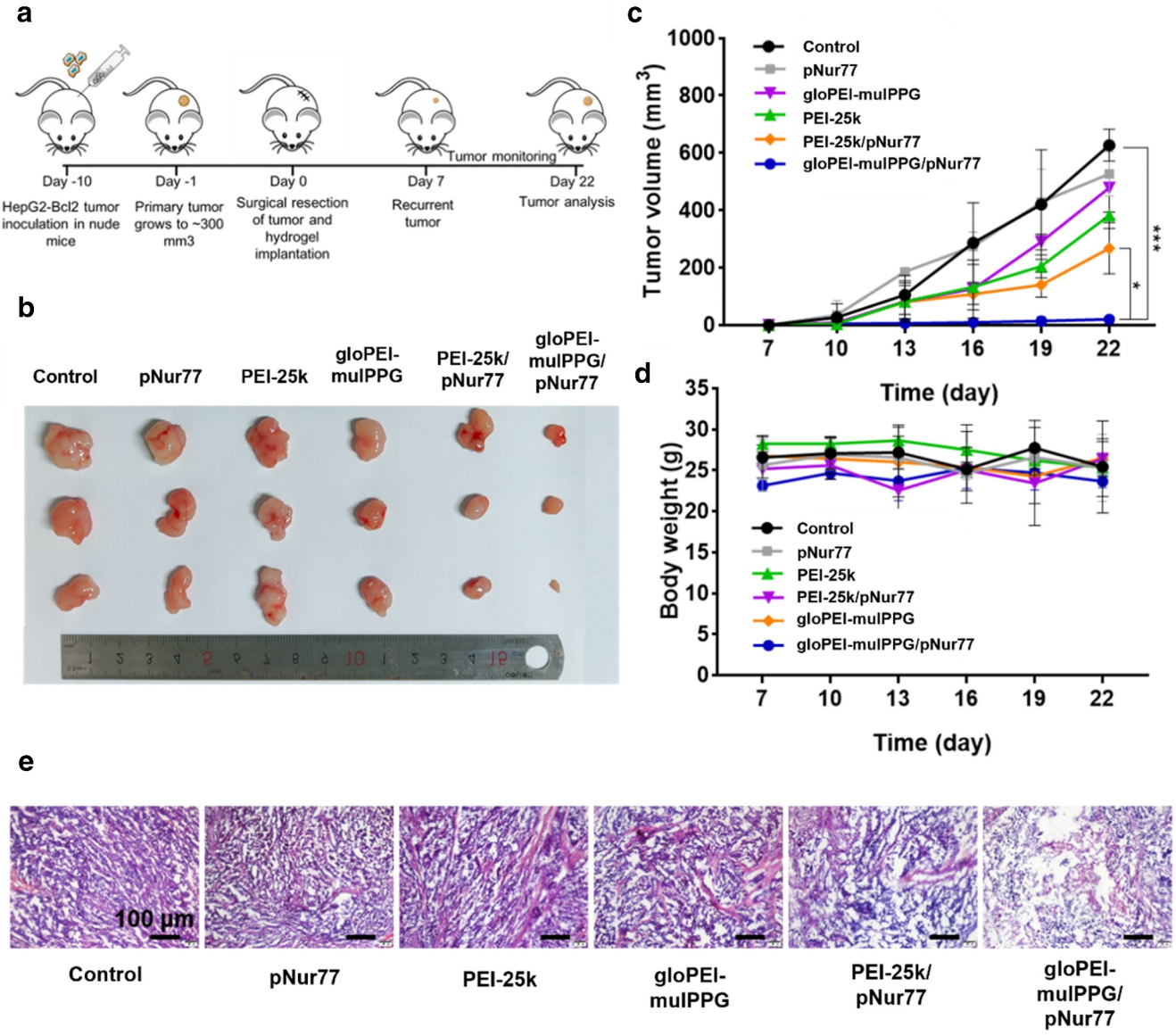

FIGURE 8 Effectiveness of various treatments at inhibiting tumor regrowth. (a) Timeline of experiment showing initial tumor growth followed by surgical removal of 98% tumor volume and application of various treatments; the rate of tumor regrowth was subsequently monitored from Day 7 to Day 22. (b) Photos of the excised recurrent tumors after the treatment period. (c) Recurrent tumor volumes and (d) Body weights of the mice models during the tumor monitoring phase. Data were plotted as mean ± standard deviation. Statistical significance was calculated by ordinary one-way ANOVA with Tukey's post hoc test, where $*p < 0.05$ and $***p < 0.001$. (e) Representative H&E images of excised tumor tissues after the various treatments. ANOVA, analysis of variance.

3 | DISCUSSION

In this work, we demonstrated an easy-to-formulate injectable single-component PEI-based thermogel gene delivery platform to combat multi-drug resistant cancer. One of the key advantages of our system is that it has comparable transfection rates as branched PEI-25 kDa gold standard. To the best of our knowledge, gloPEI-mulPPG is the first demonstration of a single component self-assembly hydrogel gene delivery platform utilizing PEI-25 kDa as the sole hydrophilic segment.[53]

GloPEI-mulPPG copolymer is a thermogelling copolymer characterized by its spontaneous micellization in water followed by micellar aggregation to form a three-dimensional supramolecular hydrogel upon warming.[40] The micellization and gelation behavior of thermogelling copolymers are driven by the dehydration of the hydrophobic segments upon warming.[54] The dehydrated and thus exposed hydrophobic segments would spontaneously coalesce to form micellar cores and micellar bridges to bring about the bulk sol-gel phase transformation.[55] To achieve this thermogelling ability,

it is essential for the copolymer to have a fine hydrophilic-hydrophobic balance; high hydrophilicity makes the copolymer too soluble to coalesce (self-assemble) while high hydrophobicity leads to precipitation of the copolymer.[36] In other words, the copolymer must be hydrophilic enough to stay soluble and hydrophobic enough to coalesce to produce the gel phase.[36] Due to the high hydrophilicity of branched PEI-25 kDa owing to its abundant nitrogen atoms capable of both protonation and hydrogen bonding, it is particularly challenging to obtain sufficient hydrophobicity when it is employed to make a thermogelling copolymer.[53] In the case of gloPEI-mulPPG, we demonstrated that with careful selection of the molecular weight and molar ratio of PPG-mbe side arms to PEI-25 kDa globular central unit, the copolymer was able to achieve sufficient dehydration of PPG-mbe side arms to exhibit sol-gel self-assembly.[56]

With its PEI content and cationic charges in gloPEI-mulPPG thermogel, it possesses similar ability as PEI to complex a high payload of genetic material.[57] Besides pNur77, we believe that our gloPEI-mulPPG thermogel is highly versatile and capable of complexing with a wide variety of genetic material by virtue of electrostatic attraction.[21] Taken together, we demonstrated that gloPEI-mulPPG thermogel is a highly facile injectable localized gene delivery platform; it only involves a single copolymer and only requires simple mixing of genetic material with its sol and spontaneous gelation will occur once injected by warming to physiological temperatures owing to its thermogelling nature.[58] In contrast, most other hydrogel gene delivery depots developed are commonly dual-component systems that require a vector to complex the genetic material and a secondary polymeric hydrogel matrix to encapsulate the gene-vector complexes to achieve localized and sustained delivery (Table 1).[59] Formulating these dual-component systems generally requires two steps, the first being complexation of genetic material to the vector and the second being embedding the complexes into a hydrogel matrix[32]; this would necessitate the optimization of both elements to achieve the desired gene release profile.[28] These dual-component systems are likely to be more challenging to prepare and optimize than our gloPEI-mulPPG thermogel single-component system.

Besides driving gelation, the non-covalent hydrophobic association within the gloPEI-mulPPG thermogel is also responsible for its ability to undergo repeated cycles of high and low strains without compromising on its original viscoelastic properties. This arises from the ability of these supramolecular interactions to form and disassemble dynamically,[60] which is not possible with covalently-crosslinked hydrogels,[61] and is key to ensure that the thermogel depot can behave in vivo as-designed after administration through injection. Additionally, our results also showed that the presence of PPG-mbe significantly improved the biocompatibility of gloPEI-mulPPG both in vitro and in vivo compared with PEI-25k. It is possible that its lowered charge density and steric hindrance provided by the PPG-mbe side-arms protected cell membranes from being disrupted by the strongly cationic PEI central unit.[62] Moreover, by being a gel with enhanced erosion resistance as compared to PEI-25 kDa solution, gloPEI-mulPPG thermogel exhibited better systemic biocompatibility where it showed lower toxicity to both the liver and kidneys. Its slower erosion allowed polymeric material to be released gradually into the bloodstream and this might have reduced in particular the burden on the kidneys.[63] Although the consumption of some of the PEI's amine groups for the PPG appendage via urethane bonds reduced the gloPEI-mulPPG copolymer's charge density compared with its PEI-25k precursor (Figure 2d), ultimately resulting in slightly reduced gene carrying capacity, the pNur77 loading achievable using our thermogels is sufficient to achieve superior therapeutic effects.

The release profile of pNur77 from the gloPEI-mulPPG showed pseudo-first order kinetics (Figure 5b), suggesting that the plasmid was released through a combination of diffusion and erosion pathways. While the exact structures of the gloPEI-mulPPG micelles remain elusive, it is reasonable to expect that the hydrophilic PEI components are exposed to the external aqueous environment that surrounds hydrophobic PPG cores. This exposes the PEI's cationic protonated amines for electrostatic complexation with the anionic pNur77 genetic material. Indeed, the complexation is strong, evident from the reduction in particle size with increasing pNur77 loading (Figure 2f). As such, pNur77 is likely to adhere to the micellar corona and be present in the inter-micellar spaces of the thermogel matrix. Due to the high concentration of pNur77 within the thermogel compared to the external physiological environment, the concentration gradient promotes pNur77 diffusion out of the thermogel depot.[64] In addition, thermogels are known to undergo surface erosion by shedding micelles from their bulk supramolecular polymeric matrix,[65] which can also elicit pNur77 release due to complexation with the shed gloPEI-mulPPG polycationic micelles. The released micelle-pNur77 complex would then be taken up by the cancer cells to achieve transfection and subsequent therapeutic effect.

4 | CONCLUSION

In summary, our results comprehensively demonstrated that the gloPEI-mulPPG cationic thermogel is highly suitable as a single-component sustained and localized gene delivery platform to combat MDR cancer. It demonstrates the key advantageous properties of facile and high payload encapsulation, minimal invasive implantation, high and sustained transfection efficiency, and minimal systemic toxicity. Its ease of formulation, coupled with its ability to possibly act as a non-viral vector for gene delivery with high loading capacity and high tolerance towards size of genetic material, potentially opens vast possibilities for targeted and localized treatment of a multitude of diseases beyond cancer.

5 | EXPERIMENTAL SECTION

5.1 | Materials

Branched PEI of 25 kDa, poly(propylene glycol) monobutyl ether (PPG-mbe) of 2.6 kDa, carbonyldiimidazole (CDI), 4-dimethylaminopyridine (DMAP), pyrene (98%), anhydrous toluene, and anhydrous dimethyl formamide (DMF) were purchased from Sigma-Aldrich. Hexane and tetrahydrofuran (THF) of high performance liquid chromatorgraphy (HPLC) grade were purchased from VWR Chemicals. Methanol of CMOS grade was purchased from J.T. Baker, Avantor. Methanol-D (CD_3OD; $D = 99.8\%$) and deuterium oxide (D_2O; $D = 99.0\%$) were purchased from Cambridge Isotope Laboratories Incorporation. Pre-wetted regenerated cellulose dialysis membrane with molecular weight cut-off of 12 kDa (Spectra/Por® 6) was purchased from Thermo Fisher Scientific. Potassium bromide for FTIR was purchased from Merck. Penicillin-Streptomycin (10,000 U/mL) antibiotics, Bicinchoninic acid (BCA) Protein Assay Kit, Dulbecco's Modified Eagle Medium (DMEM) and fetal bovine serum (FBS) were purchased from Thermo Fisher Scientific. 40,60-diamidino-2-phenylindole (DAPI) was purchased from Sigma-Aldrich. Nucleic Acid Gel Stain, Agarose, Goldview Nucleic Acid Gel Stain (100,00×), Hematoxylin and Eosin Staining (H&E) Kit, TUNEL Apoptosis Detection Kit and MTT were purchased from Yeasen Biotech. Tris base-acetic acid-EDTA buffer, DNA loading buffer, PBS and Relilla luciferase reporter kit were acquired from the Beyotime. Dimethyl sulfoxide (DMSO) was supplied by Xiamen Green Reagent Glass Instrument Co. Ltd. Anti-β-actin antibody and the secondary antibodies were provided by Cell Signaling Technology (BSN). Bcl-2 Antibody (BH3 Domain Specific) was supplied by Abcepta Biotech. Alkaline phosphatase (ALP), aspartate aminotransferase (AST), ALT, BUN and ALB detection kits were obtained from Nanjing Jiancheng Technology. Fluorescein Isothiocyanate and chloral hydrate were obtained from Shanghai Yuanye Bio-Technology. Nur77 pDNA was a Nur77 mutant as previously described.[66] GFP-labeled Nur77 pDNA was constructed by following our previous report.[67]

5.2 | Methods

5.2.1 | Synthesis of gloPEI-mulPPG thermogelling copolymer

PPG-mbe (9.0 g) was weighed into a round bottom flask (250 mL) and dissolved in anhydrous toluene (18.0 mL) at 60°C for 5 min. Two rounds of azeotropic distillation were performed on PPG-mbe to remove moisture from it. The dried slurry of PPG-mbe was loaded into a syringe. In a separate 2-neck round bottom flask (250 mL), CDI (0.585 g) was weighed out and dissolved in anhydrous DMF (4 mL) at 110°C for 5 min under argon atmosphere. DMAP (22.1 mg) was weighed out in a glass vial and dissolved in anhydrous toluene (1 mL) before being transferred to the CDI solution. PPG-mbe solution was dripped into the CDI + DMAP solution and stirred (300 rpm) at 110°C under argon atmosphere for 24 h. In a second 2-neck round bottom flask (250 mL), branched PEI (25 kDa, 5.00 g) was weighed out and dissolved in anhydrous DMF (90 mL) for 15 min at 60°C, 300 rpm, and under argon atmosphere. A glass dropper was used to transfer CDI-PPG-mbe solution into the PEI solution and this reaction mixture was stirred for 3 h at 60°C under argon atmosphere. Next, the reaction mixture was precipitated into rigorously stirred hexane (900 mL, 500 rpm) at room temperature. The crude copolymer was allowed to sediment and the supernatant was decanted. The crude gloPEI-mulPPG copolymer was further dried at 40°C under constant nitrogen gas flow with 100 rpm stirring for ~16 h and the dried product appeared as a yellow rubbery material. Crude copolymer was purified by dissolving in methanol (100 mL) at 60°C for 30 min. The copolymer methanol solution was poured into regenerated cellulose dialysis tubing with 12 kDa molecular weight cut-off and dialyzed against 5 L of deionized water for 3 days with 2 changes of water per day. Purified gloPEI-mulPPG copolymer was obtained by lyophilization and appeared as yellow rubbery material. The yield was found to be 75.6%.

5.2.2 | Molecular characterizations of gloPEI-mulPPG copolymer

The composition and absolute molecular weight of the copolymer was determined by ^{1}H NMR in CD_3OD using a Jeol 500 MHz system at room temperature. gloPEI-mulPPG was dissolved (10 mg mL^{-1}) and 64 scans were performed (Supporting Information S1: Figure S2). Chemical shifts were referred to the residual solvent peak of CD_3OD at $\delta = 3.28$ ppm. The calculations to determine composition and molecular weight are demonstrated in Supporting Information S1: Table S2. The ^{13}C NMR spectrum of gloPEI-mulPPG was obtained in CD_3OD (30 mg mL^{-1}) with 15,000 scans at room temperature (Supporting Information S1: Figure S3). Chemical shifts were referenced to the residual solvent peak at $\delta = 76.7$ ppm. Attenuated total reflectance FTIR spectra of gloPEI-mulPPG and its initial feed ingredients were obtained from 4000 cm^{-1} to 300 cm^{-1} with a resolution of 4 cm^{-1} and 64 scans using Bruker Vertex 80v (Supporting Information S1: Figure S4). DOSY was performed at room temperature on the micelle solution of gloPEI-mulPPG (1 wt%) in D_2O (Supporting Information S1: Figure S5). The optimized parameters for DOSY were as follows: relaxation delay = 6 s, diffusion time (Δ) = 0.4 s, length of gradient (δ_1) = 4 ms, maximum power gradient (G_{max}) = 0.3 mT m^{-1}, 10% of G_{max} = 0.03 mT m^{-1}, array type = logarithmic, points 32, base = 2, scans = 560. The apparent molecular weight and polydispersity index (Đ) of the gloPEI-mulPPG copolymer were determined via GPC on Agilent 1260 Infinity II (Supporting Information S1: Figure S6). The GPC system was equipped with 1260 Vial-sampler, 1260 Iso-Pump, 1260 Refractive Index Detector, and an Agilent PLgel 5 μm MiniMix-D column and Guard. The system was circulated with HPLC THF grade at 1 mL min^{-1} and 40°C. Monodispersed polystyrene standards were used to obtain a calibration curve. Copolymer samples were injected (5 mg mL^{-1}, 20 μL) for GPC measurements. Zeta potential of gloPEI-mulPPG was measured using DTS1070 cells. The micelle solution was prepared in deionized water (0.5 wt%) and the measurements were performed at 25°C in triplicates.

5.2.3 | Determination of CMC by dye solubilization method

GloPEI-mulPPG was dissolved (1 wt%, 12 mL) in deionized (DI) water before being serially diluted to obtain 12 concentrations between 0.00025 wt% and 1 wt% (4 mL per concentration). Next, pyrene was dissolved in THF at 6.0×10^{-7} M and 20 μL of this solution was added to each 4 mL copolymer solution. The THF was allowed to evaporate by leaving the copolymer solutions to air in a dark cabinet overnight. The fluorescence emission spectrum of each solution was recorded on a Shimadzu RF-5301PC spectro-fluorophotometer with excitation wavelength = 390 nm and slit width = 3.0 nm at room temperature (Supporting Information S1: Figure S7). The ratio of fluorescence intensity at 337 nm to that of 335 nm (I_{337}/I_{335}) was plotted against log(concentration). Two regions were observed on the graphs: the unimeric region at the lower concentration and the micellar region at the higher concentrations. Each region was fitted linearly and their intersection gave the CMC value.

5.2.4 | Rheological characterization of gloPEI-mulPPG thermogel

GloPEI-mulPPG was dissolved in deionized water at 4°C overnight at 10 wt%. A Discovery Hybrid Rheometer Series-3 (TA Instruments) fitted with 40 mm parallel plate geometry and a temperature-controlled Peltier base plate system was employed to probe the rheological behavior of the thermogel. In a temperature sweep experiment, the geometry gap was set to 900 μm, the strain was set to 1% within the linear viscoelastic region, the frequency was set to 1 Hz, the temperature ramp was set to 3°C min^{-1}, and the temperature range was set between 8 and 40°C. In a flow sweep rheological measurement, the shear rate was varied from 0.1 to 100 s^{-1} while the frequency was set at 1 Hz and temperature was set at 37°C (Supporting Information S1: Figure S8). In an oscillatory amplitude sweep experiment, the strain was varied from 0.1% to 1000% at a temperature of 37°C with frequency set at 1 Hz (Supporting Information S1: Figure S9). In a recovery test performed at 37°C, the frequency was set at 1 Hz and the 10 wt% gloPEI-mulPPG thermogel was subjected to 30 s of low strain (1%) followed by 30 s of high strain (500%) for a total of three cycles. In the time sweep oscillatory experiment at fixed 1% strain and 1 Hz, 10 wt% gloPEI-mulPPG was conditioned at 5°C for 100 s before being contacted with 37°C. The temperature ramp rate of the peltier plate was calculated to be 0.5°C s^{-1} (Supporting Information S1: Figure S10).

5.2.5 | Determination of temperature-concentration phase diagram

GloPEI-mulPPG was dissolved in DI water (1 mL) at concentrations ranging from 4 wt% to 14 wt% in a 4°C fridge until homogenous sols were obtained. The sols were warmed from 2 to 50°C at 2°C intervals. The samples were equilibrated for 3 min at each temperature point before being inverted for 30 s to determine if a gel

phase had formed (immobile meniscus). Their sol-gel phase transition temperatures were then recorded and plotted.

5.2.6 | Formulation of PEI-25 kDa and gloPEI-mulPPG complexes with pNur77

Nur77/DBD plasmid without DNA binding domain (pNur77) was employed as the exogeneous gene segment.[67] N/P ratio refers to the ratio of positively-chargeable amine (N) groups on the polymers to negatively-charged nucleic acid phosphate (P) groups on the gene segment. Aqueous stock solutions of gloPEI-mulPPG (5 mg mL^{-1}) and PEI-25k (1 mg mL^{-1}) were prepared. To prepare 100 μL of PEI-25k complexes with pNur77 at an N/P ratio of 20, 21 μg of PEI-25 kDa was mixed with 15 μg pNur77. Similarly, to prepare gloPEI-mulPPG (100 μL) complexes with pNur77 at an N/P ratio of 20, 60 μg of gloPEI-mulPPG was mixed with 15 μg pNur77. The mixtures were stirred for 30 min at room temperature to allow electrostatic adsorption of pNur77 onto the polymeric vectors. Furthermore, to prepare 10 wt% gloPEI-mulPPG thermogel with encapsulated pNur77, gloPEI-mulPPG (10 mg) was dissolved in 100 μL gloPEI-mulPPG/pNur77 complex solution (with N/P ratio = 20) overnight at 4°C to obtain a homogeneous sol; warming the sol to physiological temperature would cause the gel phase to form.

5.2.7 | Gel retardation test to compare the gene binding abilities of PEI-25 kDa and gloPEI-mulPPG

Increasing amounts of PEI-25k and gloPEI-mulPPG were dissolved separately into pNur77 solution (1 μg mL^{-1}) in DNA loading buffer to obtain N/P ratios ranging from 0 to 20. The polymer/pNur77 complexes were mixed for 1.5 h at room temperature before being injected via the loading mouth into 1.5% agarose gel. The electrophoresis was performed at a voltage of 100 V in 1 × TAE Buffer for 30 min. The brightness of the plasmid bands was observed under an ultra-violet image system (Bio-Rad).

5.2.8 | Particle size and zeta potential measurements

PEI-25k/pNur77 and gloPEI-mulPPG/pNur77 with N/P ratios from 0 to 20 were prepared as described in the gel retardation experiment. Each of the 100 μL polymer/pNur77 complexes was diluted to 1000 μL and allowed to equilibrate at room temperature for 30 min before their particle sizes and zeta potentials were measured at 25°C (Malvern Zetasizer, Malvern Panalytical). The scattering light angles were 15° and 90°, respectively, for particle size measurement.

5.2.9 | Measuring sustained release of pNur77 from gloPEI-mulPPG thermogel

500 μL of gloPEI-mulPPG/pNur77 complex solution with an N/P ratio of 20 was first prepared by mixing gloPEI-mulPPG (300 μg) with pNur77 (75 μg). Subsequently, 500 μL of 10 wt% gloPEI-mulPPG/pNur77 thermogel was prepared by dissolving gloPEI-mulPPG (50 mg) into the 500 μL solution of gloPEI-mulPPG/pNur77 complex solution. The gel phase was formed by warming the thermogel at 37°C for 2 min. Next, 500 μL of double distilled water was added above the thermogel and shaken at 100 rpm. 500 μL of the supernatant was removed and collected at 0.125, 0.25, 0.5, 1, 2, 3, 4, 5, and 6 days. To each of the collected supernatant, 500 μL of preheated double steam water was added before the concentration of pNur77 was quantified using a micro-ultraviolet spectrophotometer (ND1000, Thermo Fisher Scientific). The cumulative amount of pNur77 released was plotted over time.

5.2.10 | Cell culture

Human normal human kidney cells (HEK 293T) and human hepatoma cells (HepG2 cells) were obtained from American Type Culture Collection. Stable Bcl2-overexpressed HepG2-Bcl2 cell line was constructed according to the established protocol in literature.[66] All cells were cultured in DMEM supplemented with 10% FBS and 1% penicillin-streptomycin at 37°C and 5% CO_2.

5.2.11 | In vitro cell viabilities

The cell viabilities of PEI-25k and gloPEI-mulPPG, their complexes with pNur77, and eroded gloPEI-mulPPG/pNur77 from the bulk thermogel were quantified using the MTT assay. HEK 293 T, HepG2, and HepG2-Bcl2 cells were proliferated till confluence before being detached using 0.25% disodium ethylenediaminetetraacetic acid (trypsin-EDTA). The cells were separately seeded into 96-well plates with a density of 1×10^4 cells per well. After 12 h of incubation at 37°C and 5% CO_2, the old DMEM in the well plates was aspirated and replaced with solutions of the polymeric vectors or their complexes with pNur77. The samples were incubated with the cells for 24 h. Thereafter,

the samples were aspirated and replaced with MTT solution (0.5 mg mL^{-1}) diluted in DMEM before being incubated for another 3 h. Next, 150 μL of biology grade DMSO was added to each well to dissolve the blue-purple crystal methylzan. The absorption value at 490 nm of each well was quantified using a microplate reader (CMAX PLUS, Molecular Devices). Calculation of cell viability was performed according to the instructions of MTT assay's protocol.

5.2.12 | Determining transfection efficiency using pNur77-green fluorescent protein (pNur77-GFP)

HEK293T cells were seeded in 48-well plates and further cultured until they were 60%–70% confluent. PEI-25k and gloPEI-mulPPG were separately complexed with pNur77-GFP at N/P ratios ranging from 0 to 20 using the same protocol mentioned above. HEK293T cells were incubated with the complexes for 24 h before being washed gently with cold 1× PBS twice. The cells were exposed to 4% paraformaldehyde for 15 min before stained with DAPI to visualize the nuclei. A confocal laser scanning microscope system (LSM5 Exciter, Carl Zeiss Micro-Imaging) was utilized for image capture. Higher amount of green fluorescence observed was correlated with higher transfection efficiency.

5.2.13 | Determining transfection efficiency using Renilla luciferase assay

HepG2-Bcl2 cells were seeded in 48-well plates and transfected via the same protocol as the polymeric vector/pNur77-GFP mentioned above. After 24 h of incubation, the cells were lysed using the reporter lysis buffer for 30 min on an ice bath and subsequently plated in a 96-well white plate. 100 μL of Renilla luciferase reaction reagent was added to each well quickly. Luciferase reporter activity was expressed in relative light units per milligram of protein (RLU/mg protein). The amount of protein present in each well was measured using the BCA protein assay according to the manual.

AUTHOR CONTRIBUTIONS

Qianyu Lin: Data curation; formal analysis; investigation; methodology; writing—original draft; writing—review and editing. **Minting Liu**: Data curation; formal analysis; investigation; methodology; writing—original draft; writing—review and editing. **Lingjie Ke**: Data curation; formal analysis; investigation; methodology. **Nicholas Wei Xun Ong**: Data curation and formal analysis. **Joey Hui Min Wong**: Data curation and formal analysis. **Cally Owh**: Data curation; formal analysis; writing—original draft. **Valerie Ow**: Data curation and formal analysis. **Belynn Sim**: Data curation and formal analysis. **Yi Jian Boo**: Data curation and formal analysis. **Jason Y. C. Lim**: Conceptualization; supervision; writing—review and editing. **Yunlong Wu**: Conceptualization; resources; supervision; writing—review and editing; funding acquisition. **Xian Jun Loh**: Conceptualization; resources; supervision; writing—review and editing; funding acquisition.

ACKNOWLEDGMENTS

Q. Lin and J. Y. C. Lim are grateful to the IAF-PP grant (OrBiTAl: Ocular Biomaterials for Vitreoretinal Therapeutic Applications; Grant number H20c6a0033) for generous funding support; X. J. Loh acknowledges the National Research Foundation (NRF) Singapore for funding support under its NRF Investigatorship (NRF-NRFI07–2021–0003). Yunlong Wu acknowledges the generous support from Natural Science Foundation of China (82173750).

CONFLICT OF INTEREST STATEMENT

Xian Jun Loh is an editorial board member of the BMEMat journal and was not involved in the editorial review or the decision to publish this article. A patent has been filed detailing the synthesis and characterization of the PEI-PPG thermogel system, with Q. Lin, J. Y. C. Lim and X. J. Loh listed as inventors. The remaining authors declare no competing or conflicts of interest.

DATA AVAILABILITY STATEMENT

Data available in article Supporting Information S1.

ETHICS STATEMENT

The animal study was reviewed and approved by the Animal Ethics Committee of Xiamen University Laboratory, Animal Center, Xiamen University (approval number: XMULAC20230118).

ORCID

Jason Y. C. Lim https://orcid.org/0000-0002-8020-1720
Xian Jun Loh https://orcid.org/0000-0001-8118-6502

REFERENCES

1. H. Luo, C. Xu, W. Le, B. Ge, T. Wang, *J. Cell. Biochem.* **2019**, *120*, 13487.
2. T. Vos, S. S. Lim, C. Abbafati, K. M. Abbas, M. Abbasi, M. Abbasifard, M. Abbasi-Kangevari, H. Abbastabar, F. Abd-Allah, A. Abdelalim, *Lancet* **2020**, *396*, 1204.

3. F. Majolo, L. K. D. O. B. Delwing, D. J. Marmitt, I. C. Bustamante-Filho, M. I. Goettert, *Phytochem. Lett.* **2019**, *31*, 196.
4. L. Zhang, H. Zhu, Y. Gu, X. Wang, P. Wu, *J. Nanopart. Res.* **2019**, *21*, 1.
5. M. Majidinia, M. Mirza-Aghazadeh-Attari, M. Rahimi, A. Mihanfar, A. Karimian, A. Safa, B. Yousefi, *IUBMB Life* **2020**, *72*, 855.
6. S. Dallavalle, V. Dobričić, L. Lazzarato, E. Gazzano, M. Machuqueiro, I. Pajeva, I. Tsakovska, N. Zidar, R. Fruttero, *Drug Resistance Updates* **2020**, *50*, 100682.
7. A. Balmain, *Nat. Genet.* **2020**, *52*, 1139.
8. P. A. Jones, S. B. Baylin, *Cell* **2007**, *128*, 683.
9. S. A. Rosenberg, P. Aebersold, K. Cornetta, A. Kasid, R. A. Morgan, R. Moen, E. M. Karson, M. T. Lotze, J. C. Yang, S. L. Topalian, M. J. Merino, K. Culver, A. D. Miller, R. M. Blaese, W. F. Anderson, *N. Engl. J. Med.* **1990**, *323*, 570.
10. C. E. Dunbar, K. A. High, J. K. Joung, D. B. Kohn, K. Ozawa, M. Sadelain, *Science* **2018**, *359*, eaan4672.
11. M. C. Pearce, J. T. Gamble, P. R. Kopparapu, E. F. O'Donnell, M. J. Mueller, H. S. Jang, J. A. Greenwood, A. C. Satterthwait, R. L. Tanguay, X. K. Zhang, S. K. Kolluri, *Oncotarget* **2018**, *9*, 26072.
12. B. Lin, S. K. Kolluri, F. Lin, W. Liu, Y.-H. Han, X. Cao, M. I. Dawson, J. C. Reed, X.-K. Zhang, *Cell* **2004**, *116*, 527.
13. J. Thompson, A. Winoto, *J. Exp. Med.* **2008**, *205*, 1029.
14. T. Sarkar, S. Sarkar, D. N. Gangopadhyay, *Indian J. Dermatol. Venereol.* **2020**, *65*, 341.
15. E. B. Yahya, A. M. Alqadhi, *Life Sci.* **2021**, *269*, 119087.
16. J. Liu, D.-W. Seol, *BMB Rep.* **2020**, *53*, 565.
17. R. Guo, K. Li, J. Qin, S. Niu, W. Hong, *Nanoscale* **2020**, *12*, 11251.
18. C. Liu, L. Zhang, W. Zhu, R. Guo, H. Sun, X. Chen, N. Deng, *Mol. Ther. --Methods Clin. Dev.* **2020**, *18*, 751.
19. J. Yang, K. M. Luly, J. J. Green, *Wiley Interdiscip. Rev.: Nanomed. Nanobiotechnol.* **2023**, *15*, e1853.
20. N. F. Nidetz, M. C. McGee, V. T. Longping, C. Li, L. Cong, Y. Li, W. Huang, *Pharmacol. Ther.* **2020**, *207*, 107453.
21. H. Li, Z. Wang, J. Zhang, C. Yuan, H. Zhang, X. Hou, D. Zhang, *Technol. Health Care* **2019**, *27*, 263.
22. S. K. Hari, A. Gauba, N. Shrivastava, R. M. Tripathi, S. K. Jain, A. K. Pandey, *Drug Delivery Transl. Res.* **2023**, *13*, 135.
23. M. Kazemi, J. Emami, F. Hasanzadeh, M. Minaiyan, M. Mirian, A. Lavasanifar, M. Mokhtari, *Recent Pat. Anti-Cancer Drug Discovery* **2020**, *15*, 341.
24. M. Li, J. Sun, W. Zhang, Y. Zhao, S. Zhang, S. Zhang, *Carbohydr. Polym.* **2021**, *251*, 117103.
25. J. A. Duran-Mota, J. Q. Yani, B. D. Almquist, S. Borrós, N. Oliva, *ACS Biomater. Sci. Eng.* **2021**, *7*, 4347.
26. M. Enayati, W. Liu, H. Madry, R. E. Neisiany, M. Cucchiarini, *Adv. Colloid Interface Sci.* **2024**, *331*, 103232.
27. J. Zhang, Z. He, Y. Li, Y. Shen, G. Wu, L. Power, R. Song, M. Zeng, X. Wang, I. L. Sáez, *Acta Biomater.* **2023**, *8*, 48.
28. M. Ziminska, J. J. Wilson, E. McErlean, N. Dunne, H. O. McCarthy, *Materials* **2020**, *13*, 2530.
29. Ż. Słyk, R. Wrzesień, S. Barszcz, K. Gawrychowski, M. Małecki, *Biomed. Pharmacother.* **2024**, *170*, 116061.
30. S. A. Cohen, H. Simaan-Yameen, C. Fuoco, C. Gargioli, D. Seliktar, *Eur. Polym. J.* **2022**, *166*, 111038.
31. X. Fu, T. Chen, Y. Song, C. Feng, H. Chen, Q. Zhang, G. Chen, X. Zhu, *Small* **2021**, *17*, 2101224.
32. Y. J. Lu, Y. H. Lan, C. C. Chuang, W. T. Lu, L. Y. Chan, P. W. Hsu, J. P. Chen, *Int. J. Mol. Sci.* **2020**, *21*, 7111.
33. L. Ding, J. Li, C. Wu, F. Yan, X. Li, S. Zhang, *J. Mater. Chem. B* **2020**, *8*, 3527.
34. L. T. Thuy, S. Mallick, S. Kim, J. S. Choi, *Korean J. Chem. Eng.* **2023**, *40*, 325.
35. S. Dai, K. Tam, *Langmuir* **2004**, *20*, 2177.
36. Q. Lin, C. Owh, Y. C. J. Lim, P. L. Chee, P. Y. M. Yew, T. Y. E. Hor, X. J. Loh, *Acc. Mater. Res.* **2021**, *2*, 881.
37. T. M. Chapman, *J. Polym. Sci., Part A:Polym. Chem.* **1989**, *27*, 1993.
38. A. Šebenik, U. Osredkar, I. Vizovišek, *J. Macromol. Sci., Chem.* **1986**, *23*, 369.
39. L. Xu, C. Li, K. S. Ng, *J. Phys. Chem. A* **2000**, *104*, 3952.
40. S. Cui, L. Yu, J. Ding, *Macromolecules* **2018**, *51*, 6405.
41. L. Piñeiro, M. Novo, W. Al-Soufi, *Adv. Colloid Interface Sci.* **2015**, *215*, 1.
42. Y. C. J. Lim, Q. Lin, C. K. Liu, L. Guo, K. Xue, X. J. Loh, *Mater. Adv.* **2020**, *1*, 3221.
43. S. S. Liow, Q. Dou, D. Kai, A. A. Karim, K. Zhang, F. Xu, X. J. Loh, *ACS Biomater.* **2016**, *2*, 295.
44. Q. Tian, D. Zhang, N. Li, M. J. Henderson, Q. Li, G. Royal, J. R. M. Courtois, M. Yan, Z. Zhu, L. S. Almásy, *Langmuir* **2020**, *36*, 4820.
45. M. H. Butt, M. Zaman, A. Ahmad, R. Khan, T. H. Mallhi, M. M. Hasan, Y. H. Khan, S. Hafeez, E. E. S. Massoud, M. H. Rahman, S. Cavalu, *Genes* **2022**, *13*, 1370.
46. M. P. Paarakh, P. A. Jose, C. Setty, G. Peterchristoper, *Int. J. Pharm. Res. Technol.* **2018**, *8*, 12.
47. K. Kyrylkova, S. Kyryachenko, M. Leid, C. Kioussi, in *Odontogenesis: Methods and Protocols* (Ed: C. Kioussa), Humana Press, Oregon **2012**, p. 41.
48. Y. M. Kamalabadi, S. S. Sedigh, F. Fariabi, *Med. Sci.* **2020**, *24*, 1208.
49. C. F. Anyanwu, E. O. Aigbogun Jr., T. O. Joseph, *Annu. Res. Rev. Biol.* **2020**, *35*, 34.
50. D. Hwang, W. S. Lee, T. W. Goo, S. W. Park, E. Y. Yun, *Entomol. Res.* **2019**, *49*, 509.
51. X. Fang, F. Gao, Q. Yao, H. Xu, J. Yu, H. Cao, S. Li, *J. Pers. Med.* **2023**, *13*, 441.
52. P. Lu, D. Lin, N. Chen, L. Wang, X. Zhang, H. Chen, P. Ma, *Anal. Methods* **2023**, *15*, 322.
53. Q. Lin, C. C. Lim, C. Owh, J. H. M. Wong, V. Ow, B. Sim, Y. J. Boo, M. P. Yew, Y. H. Leow, L. Guo, J. Y. C. Lim, X. J. Loh, *Macromolecules* **2023**, *56*, 9368.
54. B. Q. Y. Chan, H. Cheng, S. S. Liow, Q. Dou, Y.-L. Wu, X. J. Loh, Z. Li, *Polymers* **2018**, *10*, 89.
55. S. Cui, L. Yu, J. Ding, *Macromolecules* **2019**, *52*, 3697.
56. Q. Lin, C. C. Lim, C. Owh, L. Guo, J. Y. Lim, X. J. Loh, *Mater. Today Chem.* **2024**, *38*, 102060.
57. J. Wang, H. Wang, P. Zhao, Z. Chen, Q. Lin, *Colloid Interface Sci. Commun.* **2022**, *50*, 100647.
58. C. Owh, D. J. Young, X. J. Loh, in *Thermogelling Polymers and Their History* (Eds: X. J. Loh, D. J. Young), Royal Society of Chemistry, Singapore **2018**, p. 1.
59. Z. Chen, F. Liu, Y. Chen, J. Liu, X. Wang, A. T. Chen, G. Deng, H. Zhang, J. Liu, Z. Hong, J. Zhou, *Adv. Funct. Mater.* **2017**, *27*, 1703036.
60. H. Ding, X. Liang, X. N. Zhang, Z. L. Wu, Z. Li, G. Sun, *Polymer* **2019**, *171*, 201.

61. Q. Lin, Y. C. J. Lim, K. Xue, X. Su, X. J. Loh, *Biomaterials* **2021**, *268*, 120547.
62. R. M. Kleinberger, N. A. Burke, C. Zhou, H. D. Stöver, *J. Biomater. Sci. Polym. Ed.* **2016**, *27*, 351.
63. J. E. Zuckerman, C. H. J. Choi, H. Han, M. E. Davis, *Proc. Natl. Acad. Sci. U. S. A.* **2012**, *109*, 3137.
64. D. Cao, X. Zhang, M. Akabar, Y. Luo, H. Wu, X. Ke, T. Ci, *Artif. Cells, Nanomed., Biotechnol.* **2019**, *47*, 181.
65. K. Xue, Z. Liu, Q. Lin, Y. C. J. Lim, K. Y. Tang, S. L. Wong, B. H. Parikh, X. Su, X. J. Loh, *ACS Appl. Bio Mater.* **2020**, *3*, 9043.
66. X. Liu, X. Chen, M. X. Chua, Z. Li, X. J. Loh, Y. L. Wu, *Adv. Healthcare Mater.* **2017**, *6*, 1700159.
67. X. Wang, S. S. Liow, Q. Wu, C. Li, C. Owh, Z. Li, X. J. Loh, Y. L. Wu, *Macromol. Biosci.* **2017**, *17*, 1700186.

SUPPORTING INFORMATION

Additional supporting information can be found online in the Supporting Information section at the end of this article.

How to cite this article: Q. Lin, M. Liu, L. Ke, N. W. X. Ong, J. H. M. Wong, C. Owh, V. Ow, B. Sim, Y. J. Boo, J. Y. C. Lim, Y. Wu, X. J. Loh, *BMEMat* **2025**, e70020. https://doi.org/10.1002/bmm2.70020